Dual-Piston Pressure Swing Adsorption system: Instrumentation and characterisation with pure gas experiments

Dual-Piston Pressure Swing Adsorption system: Instrumentation and characterisation with pure gas experiments

Wenli Dang, Daniel Friedrich, Stefano Brandani*

School of Engineering, University of Edinburgh, Edinburgh EH9 3JL, UK

Abstract

Dual Piston-Pressure Swing Adsorption systems offer the potential for rapid testing of novel adsorbent materials under a wide range of operating conditions. This characterisation of the properties of adsorbents is crucial for the development of efficient adsorption based separation processes. Here the instrumentation and characterisation of a semi-automated DP-PSA system as well as a mathematical model for the analysis of the experiments are presented. In this system each piston is independently controlled by a real-time computer which allows the autonomous running of a series of experiment with different cycle times, compression ratios and flow conditions. The real-time computer also handles the data acquisition from the pressure transducers (absolute and differential) and thermocouples which are placed inside the column. The entire system is enclosed in an oven to control the surrounding temperature and to enable experiments at different temperatures (20°C to 200°C). The small amount of solid material (5-10 grams) together with the possibility of fast cycle times (down to 1 Hz) allow the rapid testing of the material under a large number of different conditions. The DP-PSA is demonstrated with two series of experiments: first, empty column experiments showed that the system has a low leak rate and negligible flow resistance between the pistons and column; second, experiments with the column packed with zeolite 13X pellets to validate the mathematical model and to demonstrate the experimental procedure for pure components.

Keywords: Pressure swing adsorption; fast cycle piston driven PSA; material screening; mathematical model; kinetic and equilibrium properties

*Corresponding author E-mail: s.brandani@ed.ac.uk

1 Introduction

Pressure swing adsorption (PSA) processes are receiving considerable interest as separation route for Carbon Capture and Storage (CCS) [1], [2], for H_2 recovery from coal gas [3] and for portable oxygen generators [4]. This is due to a potentially lower energy consumption and lower capital costs compared to other separation processes. For example, in comparison to the first generation of CO_2 capture plants, which use liquid absorbents such as MEA, separation of CO_2 by a PSA process has the potential of higher productivity and a lower specific energy consumption [1], [5].

To push PSA technology to its limit of productivity, ie process intensification, rapid cycling is an essential target, but it is difficult to test novel materials under such conditions. For this purpose a new total recycle dual piston PSA system has been developed. This system is a variant, with no product withdrawal, of the dual piston PSA (DP−PSA) process developed originally by Keller and Kuo in 1982 [6]. The apparatus can also be seen as a new development in closed system frequency response (FR) adsorption measurements based on perturbations of the system's volume [7], [8], which have been further developed to include step changes in volume [9]; measurement of thermal FR [10]; and extensions to nonlinear responses [11]. These FR approaches are all based on small volume changes, typically a few percent at most (7% maximum in the case of the non-linear system) and the samples are normally small batches of a few mg. Here the sample is packed as a normal adsorption column thus allowing to characterise not only mass transfer resistance and equilibrium properties, but the full range of physical parameters required to model an adsorption column including heat transfer resistances and pressure drop correlations in a reversing flow apparatus. As a FR system it has also an advantage over the flow systems based on concentration FR [12], [13] and pressure FR [14] that the experiment does not consume large quantities of gas and that it operates with reversing flows, which are typical in PSA cycles [15].

The interpretation of the results from the DP-PSA system requires sophisticated models due to the dynamic nature of the process. A non-isothermal model was presented by Singh and Jones [16]. This model uses an iterative trial and error approach for the system pressure and neglects the pressure drop along the column. Furthermore, it uses the plug flow model so that the axial mass and energy dispersion are only approximated by numerical dispersion. Soon afterwards, Farooq et al. [17], [18] developed a numerical model which simultaneously calculated the pressure with the other system variables, i.e. gas composition, flow rate and adsorbed concentration, and included axial dispersion. However, the model is isothermal and neglects the column pressure drop. Nevertheless the model showed good agreement with the experimental runs and allowed the investigation of the separation performance. It was shown that for faster cycles mass transfer resistance becomes critical. Friedrich et al. [19], [20] extended the model of Farooq et al. by adding the Ergun pressure drop model, non-isothermal operation as well as micro- and macropore diffusion models. In addition, they present a number of acceleration schemes which can decrease the simulation time to reach cyclic steady state (CSS) by an order of magnitude.

In this publication the development and operation of a semi-automatic DP-PSA system for the characterisation of adsorbent materials is presented. First, the design, instrumentation and experimental characterisation of the DP-PSA system itself as well as the Labview control software are described in detail. This is followed by a series of experiments which demonstrate the procedure and capabilities of the DP-PSA system for the characterisation of adsorbents. Finally, the numerical model developed for the analysis of the DP-PSA experiments is presented and compared to the experiments with pure gases on zeolite 13X.

2. Experimental apparatus and procedure

A schematic diagram of the experimental system is shown in Figure *1* and the system dimensions are given in Table 1. The main parts of the system are the two computer controlled pistons, Ps1 and Ps2, which are

connected to the top and bottom of the adsorption column, AC. The auxiliary parts are the surrounding oven, the dosing system, the pressure and temperature sensors and the real-time controller. From now on the part of the system to the right of valve V8, i.e. the adsorption column and the two pistons, are termed the *column side* while the part to the left of valve V8 is termed the *feed side*. An annotated picture of the DP-PSA system is shown in Figure *2*.

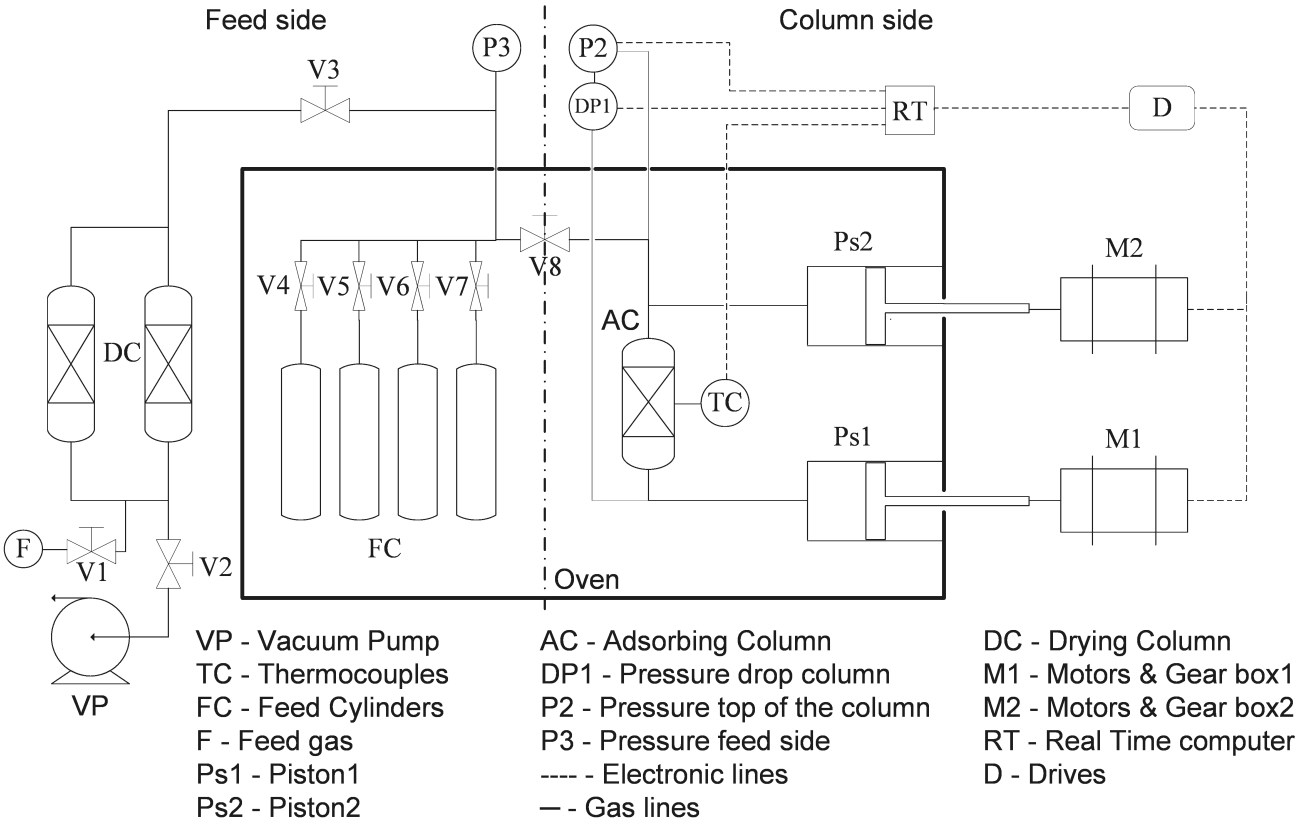

Figure 1: Schematic of the DP-PSA system. The part of the system left of valve V8 will be called *feed side* while the part right of valve V8 will be called *column side*.

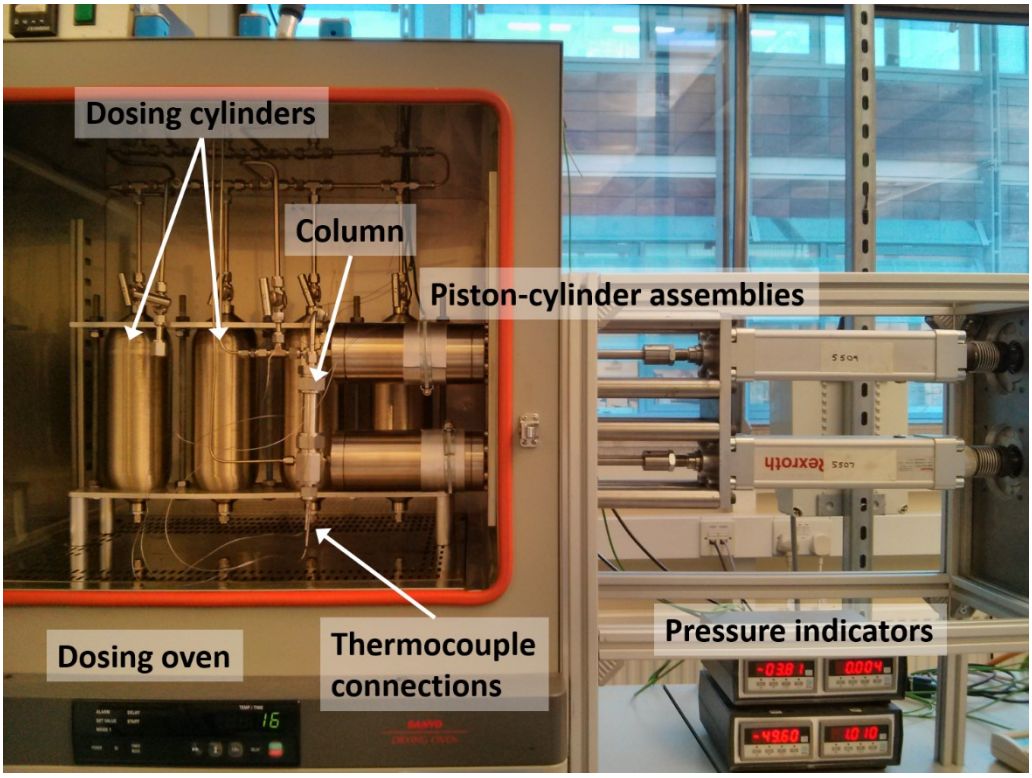

Figure 2: Annotated picture of the DP-PSA system.

2.1 Piston-Cylinder assembly

The two piston-cylinder assemblies were fabricated in the university workshop to fit inside the oven. The seals of the piston-cylinder assembly are designed to work at pressures between 0.001 bar and 20 bar and up to 260 ˚C; thus allowing Vacuum Swing Adsorption (VSA) and PSA experiments.

Table 1: DP-PSA system dimensions

Description	Parameter	Value	Unit
Piston radius	r_{pi}	0.025	m
Piston stroke length	L_{pi}	0.11	m
Cylinder wall thickness		0.0125	m
Piping radius		0.0025	m
Bottom piping length	L_{p1}	0.12	m
Top piping length	L_{p2}	0.09	m
Column radius	r_c	0.0078	m
Column length	L_c	0.13	m
Column wall thickness		0.005	m
Specific heat of column/piston wall	$c_{P,w}$	500	J kg^{-1} K^{-1}
Column/piston wall density	ρ_w	8238	kg m^{-3}

The pistons are driven by AC motors through a linear motion gearbox (Bosch Rexroth AG, R156030000). The AC motors are controlled by two independent ACSM1 drives from ABB, which in turn are controlled through the real-time computer, see section 2.4. In this configuration the two pistons are totally independent thus they can run cycles with different conditions. The ABB drives are controlled through a LabVIEW interface which allows

the configuration of the cycle duration, start and end positions, starting phase angle and experiment duration. In this contribution the cycle shapes are sinusoidal which generates a smooth cyclic process similar to the previously reported DP-PSA systems [16]–[18]. However, the piston routes can be programmed to any shapes, e.g. ellipsoid or linear. The cycle duration can be set between 0.5s and tens of minutes; thus allowing the testing of different time constants. Hereinafter the piston-cylinder assembly is referred to as the *piston*.

The start, S_0, and end, S_1, positions of the cycle as well as the starting phase angle, φ, of the pistons are shown in Figure 3. The difference in starting phase angle between the two pistons, i.e. $\varphi=\rho_{Ps1}-\rho_{Ps2}$, defines the operation of the DP-PSA system. For φ=0 the two pistons are in-phase, i.e. they move at the same time either towards or away from the column. In this case the system experiences the highest compression ratio but for an equal stroke length in both pistons there is no flow across the entire adsorbent column, i.e. for half the cycle gas is flowing into the column from both ends and for the other half gas is leaving the column at both ends. For φ=π the two pistons are out-of-phase, i.e. one piston is moving towards while the other is moving away from the column. For an equal stroke length in the two pistons the system has constant volume and thus no compression or expansion takes place.

The cycle time, piston start and end positions and the phase angle define the operational profile and influence the performance of the adsorption cycle. For example, the piston strokes and phase angle define the flow conditions and pressure profiles over the cycle. It is well known that these in turn influence the performance, e.g. purity, recovery and specific energy, of the adsorption separation process. In addition, the cycle time will strongly affect the productivity and specific energy of the separation process. However, the interplay between the operating variables and the separation process is very complex and beyond the scope of this manuscript.

2.2 Adsorption column

The adsorption column is placed between the two pistons. The current column dimensions can be found in Figure 3 and Table 1. However, columns of different length and diameter can be used to generate the desired experimental conditions, e.g. a smaller column can be used for experiments with higher compression ratios. The *column side*, i.e. the adsorption column and the two pistons, is separated from the *feed side* by valve V8. Thus during experiments the system is closed and run at total reflux.

An absolute pressure transducer, P1, (0-3.5 bar; precision 1 mbar, Drück PDCR 4701) and a differential pressure transducer P2, (–0.5-0.5 bar; precision 0.2 mbar, Drück PDCR 4701) are connected to the adsorption column. Both pressure transducers are connected to a Drück DPI 280 series process indicator with serial interface. The inner diameter of the connecting lines is 5 mm and the length of the piping is LP1≈0.09 m and LP2≈0.12 m. Four type K thermocouples are arranged in pairs inside the column as shown in Figure 3. One thermocouple from each pair is inserted into an adsorbent pellet which allows the measurement of the adsorbent temperature while the other thermocouple is in the gas phase. A further thermocouple of the same type is placed just outside of the column to monitor the temperature inside the oven. This will allow correction for any temperature fluctuations inside the oven.

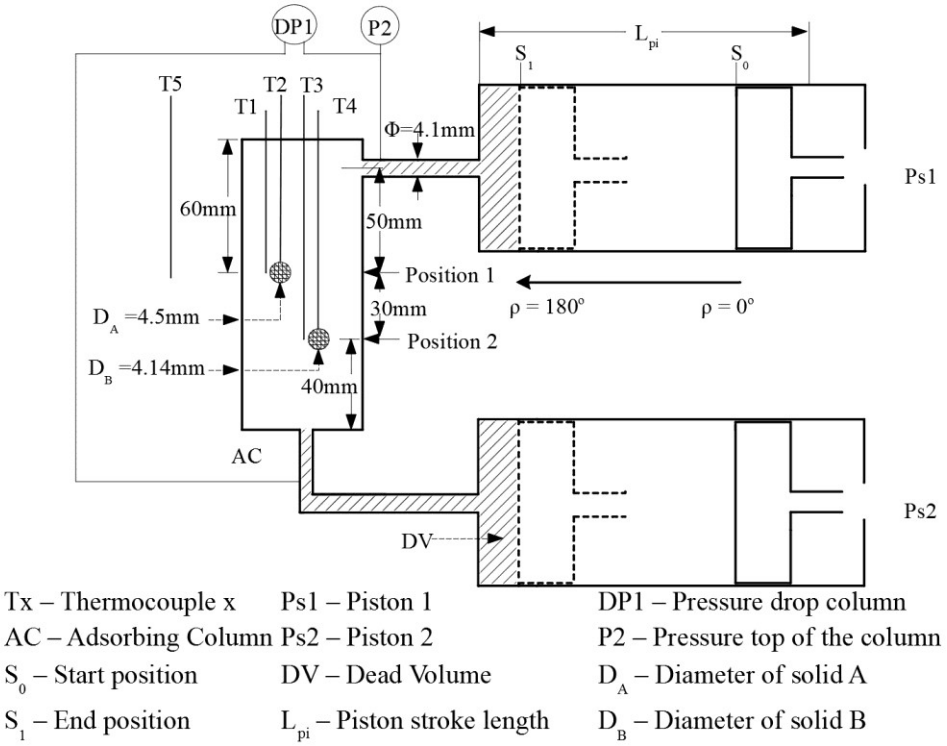

Figure 3: Schematic of the adsorption column and the two pistons showing the dimensions of the system and the locations of the thermocouples and pressure transducers.

2.3 Oven and dosing system

The pistons, the adsorption column and the feed cylinders are enclosed in an oven (Sanyo MOV-112). This oven which can reach a maximum temperature of 260 °C ensures that all parts of the system have the same initial temperature and almost constant surrounding conditions. The piping inside the oven is separated from the piping outside by valve V3; see Figure 1.

The dosing system consists of drying columns connected to CO_2, N_2 and He lines, an Edwards XS5 oil-free vacuum pump and 4 cylinders of exactly 1 litre. The drying columns ensure that the feed gas entering the DP-PSA system is as dry as possible; this is necessary since humidity can have a profound effect on the adsorbent material, e.g. reducing the capacity. The vacuum pump is required for the evacuation of the system and together with the oven set to a high temperature for the regeneration of the adsorbent. The 4 feed cylinders are used for the preparation of feed gas. While in this contribution only single component experiments are reported the system can be used to prepare multi-component gas mixtures, including vapours such as water, and this is described in Hu et al. [21] The pressure transducer, P3, (0-3.5 bar; precision 3.5 mbar, Drück PDCR 5010) is used to measure the amount of gas dosed into the column side.

2.4 Control instrumentation

A Compact RIO 9022 real-time computer, RT, from National Instrument (NI) is employed to facilitate accurate control of the piston movement and high frequency data logging. The real-time computer communicates with the ABB drives through 2 different NI modules: a serial interface module, NI9871, is used to configure the drive at the start of the experimental run, i.e. setting the speed, acceleration and deceleration of the motor, and to record the actual piston position during the experiment; an analog output module, NI9263, is used to control the positions of the pistons during the experiment. The use of an analog module is required for the control of fast cycles, i.e. cycle durations below 10 s, due to the high latency in the serial interface module. The pressures are recorded through a serial interface module, NI9870, and the temperatures from the five thermocouples are recorded through a thermocouple input module, NI9213.

2.5 Software design

The user interface, control and data logging are programmed in the NI LabVIEW environment on a PC. The user interface allows the configuration of a series of experiments, i.e. a number of experiments with different cycle configurations such as stroke length or cycle duration. Once the cycle configurations are specified the code is uploaded to the Compact RIO. From this point on the real-time computer controls the pistons and data logging independently of the development PC. After the series of experiments is finished the recorded data can be transferred to the PC for analysis.

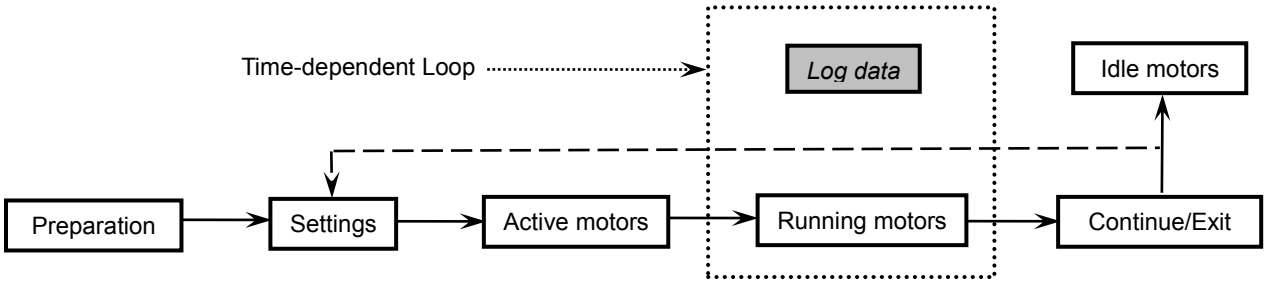

Figure 4: Software control structure

To increase the communication speed, the FPGA (Field-Programmable Gate Array) between the real time computer and functional modules, e.g. serial interface module, is used for the configuration and control of the system. The DMA (Direct Memory Access) FIFO (First In, First Out) method is applied to achieve fast and efficient communication. The DMA method does not involve the host processor and it is therefore the fastest available method for transferring large amounts of data between the FPGA target and the host. It also frees the host processor to perform other calculations during data transfer and automatically synchronises data transfers between the host and the FPGA target.

The FPGA configuration code is implemented as a parallel structure for each function, thus all data logging and piston control is performed simultaneously with minimum delay (<1 ms). The DP-PSA control code is modularised into seven code blocks which are shown in Figure 4. In the *Preparation* module at the start of the program the parameters of the motor, i.e. position and velocity reference, are set to safe default values. Based on the user's cycle configuration parameters, the acceleration, deceleration and speed settings of the motors are calculated in the *Settings* module and transferred via a serial link to the ABB drivers. Then the motors are activated and the pistons are moved to their initial positions. Once the pistons are in the starting positions the system is run for the specified runtime and with the specified cycle configuration. During the running of the experiment, the actual piston positions, the two pressures and the five temperatures are read continuously

with a fixed frequency and written to the log files. Once the runtime for this experiment is reached, the code identifies if there is still an experiment in queue. If there is a further experiment the code moves to the next set of experimental parameters and goes back to the Settings module. Otherwise, the pistons are moved to the initial safe conditions and the motors are set to idle.

2.6 Experimental procedure

The computer-control of the piston movement and data logging allows the semi-automated running of a series of experiments. However, several steps have to be manually performed to prepare the system for a series of experiments. These steps are in the order they have to be performed:

i) preparation of the gas mixture,
ii) regeneration of the adsorbent,
iii) setting of the oven temperature.

The gases are prepared in the feed cylinders inside the oven before the regeneration of the adsorbent. The adsorbent material inside the column has to be regenerated, i.e. adsorbed gas or water molecules have to be desorbed, before each new series of experiments. For the zeolite 13X pellets used in this study the oven temperature is set to 200 °C and the system is evacuated by the vacuum pump for at least 12 hours. At the end of the regeneration period the oven temperature is set to the desired temperature while maintaining the vacuum. While the oven cools down to the experimental temperature the two pistons are moved in a slow cycle (t_c=40 s) and out-of-phase. This ensures that the pistons are at a uniform temperature while keeping the volume in the system constant. Once the system reaches the set temperature, which can be monitored through the thermocouples inside the column, the gas mixture is fed into the *column side*.

The procedure for feeding the gas is as follows: the required pure gas is prepared in the feed cylinders in advance; the pressure on the *feed side* is recorded; the valve connecting the cylinders and the column is opened to feed the gas into the *column side* of the system; after closing the feed valve the pressure on the *feed side* is recorded again. The pressure at the *feed side* before and after feeding the gas into the column allows the calculation of the number of gas molecules inserted through an equation of state. The preparation and feeding of mixtures, also including vapours, is described in Hu et al. [21].

Once the system temperature and pressure have stabilised the series of experiments is started. Since the oven is not controlled through the LabVIEW interface each series of experiments is typically run at one temperature. The parameters of the experiments are passed to the real-time computer which runs the experiments in a sequential way (see Section 2.5). Between individual experiments the pistons are kept moving with the same cycle duration of the previous experiment but with the pistons in the out-of-phase configuration.

3. Mathematical model

A mathematical model describing the mass, momentum and energy balances in the DP-PSA system was developed and presented in a previous publication [20]. Briefly, the governing equations for the pistons and the column will be described separately and linked together through boundary conditions. The connecting pipes are modelled as empty columns. The models are based on the following assumptions:

1. Axial dispersed plug flow
2. Momentum balance: pressure drop described by the Ergun equation
3. Energy balance: non-isothermal model with three non-constant temperatures: fluid temperature T_f, pellet temperature T_p and wall temperature T_w
4. Mass transfer: macropore Linear Driving Force (LDF) and micropore LDF
5. Adsorption isotherm: dual-site Langmuir

6. The gas concentrations and temperature in the pistons are assumed to be uniform
7. The dead volume in the system is placed at the top of the pistons
8. Flow resistance between the pistons and the column

In contrast to the model presented in [20], the dual-site Langmuir isotherm is used and the energy balance considers varying column wall temperature as well as enthalpy change in the adsorbent pellets due to mass diffusion. Furthermore, the heat transfer into the thermocouples is considered as described further down.

3.1 Governing equations for the column

Since the flow is assumed to be dispersed plug flow the material balance along the column is given by

$$\frac{\partial c_i}{\partial t} + \frac{(1-\varepsilon)}{\varepsilon} \cdot \frac{\partial \bar{Q}_i}{\partial t} + \frac{\partial (c_i \cdot v)}{\partial z} + \frac{\partial J_i}{\partial z} = 0 \quad (1)$$

$$\bar{Q}_i = \varepsilon_p c_{m,i} + \left(1-\varepsilon_p\right)\bar{q}_i \quad (2)$$

$$J_i = -D^L c_T \frac{\partial x_i}{\partial z} \quad (3)$$

Here and from now on the index i goes from 1 to the number of components$N$. While this manuscript considers only pure gases (i.e. $N = 1$), the model is written for gas mixtures which will be considered in a future publication. The mass transfer in the macro- and micropores is given by

$$\varepsilon_p \frac{dc_{m,i}}{dt} + \left(1-\varepsilon_p\right)\frac{d\bar{q}_i}{dt} = k_i^p \frac{A_p}{V_p}\left(c_i - c_i^m\right) \quad (4)$$

$$\frac{d\bar{q}_i}{dt} = k_i^{cr} \frac{3}{r_{cr}}\left(q_i^* - \bar{q}_i\right) \quad (5)$$

where q_i^* is the sorbate concentration in the adsorbent crystal at equilibrium. This value depends on the used adsorption isotherm. Here the dual-site, multi-component Langmuir isotherm is used

$$q_i^* = \frac{q_s^1 b_i^1 P x_i}{1+\sum_{j=1}^N b_j^1 P x_j} + \frac{q_s^2 b_i^2 P x_i}{1+\sum_{j=1}^N b_j^2 P x_j} \quad (6)$$

with $b_i^l = b_{i,0}^l \, exp\left(\frac{-\Delta H_i^l}{RT}\right)$.

The energy balance in the column is written in terms of the internal energy in the fluid and pellet plus a term for the column wall temperature

$$\varepsilon \frac{\partial \breve{U}_f}{\partial t} + (1-\varepsilon)\frac{\partial \breve{U}_p}{\partial t} + \varepsilon \frac{\partial (\breve{H}_f \cdot v)}{\partial z} + \frac{\partial J_{th}}{\partial z} + \sum_{i=1}^N \frac{\partial (J_i \tilde{H}_i)}{\partial z} + h_w \frac{A_c}{V_c}\left(T_f - T_w\right) = 0 \quad (7)$$

$$\frac{d\breve{U}_p}{dt} = \varepsilon_p \frac{d\breve{U}_m}{dt} + \left(1-\varepsilon_p\right)\frac{d\breve{U}_{cr}}{dt} = h_p \frac{A_p}{V_p}\left(T_f - T_p\right) + \frac{V_p}{A_p}\sum_{i=1}^N \frac{\partial \bar{Q}_i}{\partial t}\tilde{H}_i \quad (8)$$

$$\rho_w \hat{c}_{P,w} \frac{dT_w}{dt} + h_w \frac{A_{c,i}}{V_w}\left(T_w - T_f\right) + U \frac{A_{c,e}}{V_w}\left(T_w - T_\infty\right) = 0 \quad (9)$$

$$J_{th} = -\lambda_f^L \frac{\partial T_f}{\partial z} \quad (10)$$

The pressure in the system is calculated from the gas phase concentration and temperature through the ideal gas law. The interstitial flow velocity v is calculated from the Ergun equation

$$-\frac{\partial P}{\partial z} = \frac{150\mu(1-\varepsilon)^2}{4r_p^2\varepsilon^2} v + \frac{1.75\rho_f(1-\varepsilon)}{2r_p\varepsilon} v|v| \quad (11)$$

which has been shown to accurately describe the pressure drop in adsorption processes [22].

3.2 Column boundary and initial conditions

The boundary equations for the mass and energy balance in the column are given by the Danckwert's boundary conditions which can be written concisely for reversing flows as

$$J_{th}|_{z=0} = \frac{v+|v|}{2}\left(\breve{H}_{f,0-} - \breve{H}_{f,0}\right) \quad (12)$$

$$J_{th}|_{z=L_c} = \frac{v-|v|}{2}\left(\breve{H}_{f,L_c+} - \breve{H}_{f,L_c}\right) \quad (13)$$

$$J_i|_{z=0} = \frac{v+|v|}{2}\left(c_{i,0-} - c_{i,0}\right) \quad (14)$$

$$J_i|_{z=L_c} = \frac{v-|v|}{2}\left(c_{i,L_c+} - c_{i,L_c}\right) \quad (15)$$

The velocities at the column boundaries are calculated from the resistance term between the pistons and the column. Initially the column is at uniform pressure, temperature and gas phase concentration. The adsorbent material is assumed to be in equilibrium with the set gas phase concentration. The uniform initial pressure and adsorbed concentration can be calculated by solving the mass balance between the number of moles in the system and the number of moles in the gas and solid phase. In the experimental system the initial conditions might not be perfectly uniform, but this has no impact on the cyclic steady state of the system as long as the mass balance is correct which is ensured by the uniform initial conditions.

3.3 Governing equations for the piston

In the current study each piston performs a sinusoidal cycle and can thus be described by the following equation

$$S(t) = S_0 + \frac{S_1 - S_0}{2}(1 - cos(\omega t + \phi)) \quad (16)$$

where S_0 and S_1 are the start and end position of the piston, respectively, $\omega = 2\pi/t_c$ is the cycle frequency and ϕ the initial piston offset. The material balance in the pistons is given by

$$\frac{d(c_i V)}{dt} = \frac{F+|F|}{2}\frac{c_{i,n}}{c_{T,n}} + \frac{F-|F|}{2}\frac{c_i}{c_T} + f(t) \quad (17)$$

where $f(t)$ characterises the leak of the piston and the subscript n indicates the concentration in the neighbouring unit, i.e. the connecting pipes. The flow rate at the piston outlet is modelled through a resistance term

$$F = \kappa(P_n - P) \quad (18)$$

The energy balance is written in terms of internal energy plus an equation for the wall temperature

$$\frac{dU_f}{dt} = F\widetilde{H} - P\frac{dV}{dt} - A_c h_w\left(T_f - T_w\right), \quad (19)$$

$$\rho_w \hat{c}_{P,w}\frac{dT_w}{dt} = h_w\frac{A_{c,i}}{V_w}\left(T_f - T_w\right) + h_w\frac{A_{c,o}}{V_w}\left(T_{\infty,o} - T_w\right) + U\frac{A_{c,e}}{V_w}\left(T_\infty - T_w\right) \quad (20)$$

Here the terms on the right hand side are the heat transfers to the piston wall. The first two terms are the heat transfer from the inside of the piston to the piston wall; the terms $A_{c,i}$ and $A_{c,o}$ give the surface area inside and outside of the closed DP-PSA system and depend on the piston stroke position. The third term is the heat transfer from the oven to the outside of the piston and depends on the external surface area of the piston$A_{c,e}$.

3.4 Numerical solution

The governing partial differential algebraic equations are solved with the Method of Lines. Here the spatial dimension is discretised in space using a flux-limited finite volume method [19] and the resulting set of ordinary differential algebraic equations is integrated in time with the variable time step, variable order backward differentiation formulas implemented in SUNDIALS [23].

4 Experiment and simulation parameters

It is clear from the mathematical model in section 3 that the performance of the DP-PSA system depends on a large number of parameters. It is not feasible to estimate all parameters from DP-PSA experiments and indeed many parameters can be determined with independent experiments or estimated from established correlations.

4.1 Adsorbent

Spherical zeolite 13X pellets (APG MOLSIV™) from UOP, a Honeywell company, are used in this study as the adsorbent material. This material has a large working capacity for CO_2 compared to its capacity for N_2 and He and is macropore diffusion limited [24], [25]. The parameters for the adsorption of CO_2 and N_2 and the physical properties of zeolite 13X are listed in Table 2.

Table 2: Adsorbent parameters and physical properties of zeolite 13X. The superscript indicates the adsorption site and the subscript the adsorbate: 1 for CO_2 and 2 for N_2

Description	Parameter	Value	Unit
Dry adsorbent mass		13.1	g
Pellet radius	r_p	0.002	m
Pellet void fraction	ε_p	0.25	
Pore radius	r_{pore}	10^{-7}	m
Tortuosity	τ	3	
Specific heat at constant temperature		1339	J kg^{-1} K^{-1}
Adsorbent crystal density		1403	kg m^{-3}
Equilibrium capacity site 1	q_s^1	3.44	mol kg^{-1}
Equilibrium capacity site 2	q_s^2	2.20	mol kg^{-1}
Langmuir constant for CO_2 site 1	$b_{1,0}^1$	2.93×10^{-5}	bar^{-1}
Langmuir constant for CO_2 site 2	$b_{1,0}^2$	3.83×10^{-5}	bar^{-1}
Langmuir constant for N_2 site 1	$b_{2,0}^1$	5.29×10^{-6}	bar^{-1}
Langmuir constant for N_2 site 2	$b_{2,0}^2$	2.78×10^{-5}	bar^{-1}
Heat of adsorption for CO_2 site 1	ΔH_1^1	30031	J mol^{-1}
Heat of adsorption for CO_2 site 2	ΔH_1^2	37449	J mol^{-1}
Heat of adsorption for N_2 site 1	ΔH_2^1	19752	J mol^{-1}
Heat of adsorption for N_2 site 2	ΔH_2^2	21504	J mol^{-1}
Effective macropore diffusivity for CO_2	$D_{p,1}^e$	2.7×10^{-6}	m^2 s^{-1}
Effective macropore diffusivity for N_2	$D_{p,2}^e$	3.2×10^{-6}	m^2 s^{-1}

The adsorption isotherms for CO_2 and N_2 were measured on a Quantachrome Autosorb and were previously reported [24]. The experimental data is fitted with the dual-site Langmuir isotherm. Since the mass transfer mechanism of CO_2 and N_2 in zeolite 13X is macropore diffusion controlled, the adsorbed phase in the micropores is at equilibrium with the gas in the macropores. This is approximated by using a large micropore mass transfer coefficient k_i^{cr} in the simulations. The LDF coefficient for the macropores k_i^p which determines the adsorption kinetics can be calculated from the diffusivities in the macropore [5]. Briefly, for the pure gas experiments in this contribution the effective macropore diffusivity is given by

$$D_{p,i}^e = \frac{\varepsilon_p}{\tau}\left(D_i^K + D_i^v\right) \tag{21}$$

where D_i^K and D_i^v are the Knudsen diffusivity and the viscous flow for component i, respectively. Due to the dynamic nature of the DP-PSA system and adsorbent systems in general these values vary during the operation of the adsorbent process. A reasonable estimation is given by using the average temperature and pressure of the process. The values used for the simulations are given in Table *2*.

4.2 Column heat and mass transfer parameters

It was shown in a previous publication [20] that it is crucial to use a non-isothermal model for cycle configurations with cycle times below around 10 seconds. The accuracy of the non-isothermal model depends

on the accuracy of the adsorbent properties and the heat transfer coefficients. The adsorbent properties were given in the last section and here the heat transfer coefficients for the piping, column and pellets are given below.

The heat transfer coefficient h_x can be written in terms of the Nusselt number

$$h_x = \frac{kNu_x}{2r_x} \quad (22)$$

where $k$is the thermal conductivity, Nu_x and r_x are the Nusselt numbers and radii, respectively, for the relevant geometry x. The Nusselt numbers for the empty bed, i.e. $\epsilon \approx 1$, are given by the correlations for heat transfer for flow around a sphere and flow in a pipe for the pellet and column, respectively, [26], [27]

$$Nu_p = 2 + \left(0.4Re_p^{0.5} + 0.06Re_p^{2/3}\right) Pr^{0.4}, \qquad \epsilon \approx 1 \quad (23)$$

$$Nu_c = 1.86\left(Re_c Pr \frac{2r_c}{L_c}\right)^{1/3}, \qquad \epsilon \approx 1 \quad (24)$$

For the packed bed the Nusselt number for the pellet is given by the Wakao correlation [28]

$$Nu_p = 2 + 1.1Pr^{1/3}Re_p^{0.6} \quad (25)$$

and the Nusselt number for the column is calculated from a correlation given by Li and Finlayson [29]

$$Nu_c = 2.03Re_p^{0.8}\left(e^{6r_p/r_c}\right)^{-1} \quad (26)$$

The Nusselt number for the connecting pipes is calculated from the correlation for heat transfer in a pipe. The Reynolds numbers for the different sections are defined in the appendix. These Nusselt numbers are for steady turbulent flow while the flow in the DP-PSA is oscillating. It has been reported that for oscillating turbulent flows the heat transfer coefficients can be up to 5 times higher [30]. The reason for this are not fully understood but are thought to be due to the flow reversal and to entrance effects at both sides of the system. For the packed column runs with small cycle times (less than 10 seconds) the calculated Nusselt numbers were increased by 20% to match the temperature profiles.

Initial comparisons between experimental data and the simulation showed that the kinetics of the heat transfer in the thermocouple need to be taken into account. The response of the thermocouples inside the column can be calculated from the simple first order relationship

$$\frac{dT_{TC}}{dt} = \frac{h_{TC}A}{V\rho\hat{c}_P}\left(T_p - T_{TC}\right) \quad (27)$$

where T_p is the simulated temperature in the surrounding adsorbent pellet. The resulting thermocouple temperature T_{TC} should match the experimental temperature. The temperature response for the thermocouples in the gas and solid phase was very similar which suggests that the gas phase thermocouples are in contact with the outer surface of the solid pellets. This is feasible due to the tight packing. The heat transfer from the solid pellet to the thermocouple is dominated by the heat conductivity of the solid. The heat conductivity for zeolite 13X was given as 0.2 W m^{-1} K^{-1} [31]. For the given pellet radius this results in a heat transfer coefficient of $h_{TC} = 100$ W m^{-2} K^{-1}.

The axial dispersion coefficient $D_Z$and the axial thermal coefficient$\lambda_z$can be approximated with the following equations [28], [32]

$$D^L = \frac{D_i^m}{\varepsilon}(20 + 0.5Sc\,Re) \quad (28)$$

$$\lambda_f^L = k(7 + 0.5\,PrRe) \quad (29)$$

Here Sc and Pr are the Schmidt and Prandtl numbers, respectively.

5. System characterisation experiments

Before the system can be used to analyse novel adsorbents it is crucial to characterise the DP-PSA system and

to validate the mathematical model. Several experiments were run with the empty DP-PSA system to achieve this. These experiments are used to characterise the system with respect to the dead volume, leak rates and resistance in the lines connecting the pistons to the column. An accurate characterisation of these is important for the fitting of simulations to the experimental results. As shown in Figure 3 the column contains two zeolite 13X pellets and thus is not completely empty. However, the void fraction of the column is ~0.996 and thus the effect of these two pellets on the column pressure and temperature will be negligible even for a strongly adsorbing gas such as CO_2. All the experiments are run with the feed valve V8 closed and thus at total reflux.

5.1 Cycle shapes

In contrast to the previously reported DP-PSA systems [16]–[18] the piston movement is not inherently sinusoidal but can take almost any shape. However, for the initial tests a sinusoidal cycle shape was chosen. This cycle produces a smooth change of the pressure and flow velocities in the system and allows the comparison with previously reported results. The combination of digital and analog communications (see Section 2.4) allows accurate control of the cycle shape down to cycle durations of less than 1 second. The RMS error between the calculated piston position and the actual, measured piston position over one cycle is about 1% of the stroke length.

5.2 Piston and dead volumes of the system

First the volume V_{V3-V8} of the piping from valve V3 to valve V8 is measured. This is accomplished by filling one of the feed cylinders with a known amount of helium which is assumed to be non-adsorbing; evacuating the piping between V3 and V8; opening the feed cylinder and recording the pressure. Since the amount of gas, the temperature and the pressure are known the volume of the piping can be calculated from the ideal gas law. Five tests have been performed and the average volume is $V_{V3-V8} = (4.24 \pm 0.05) \cdot 10^{-5} m^3$.

The volumes on the *column side* are measured in the following way. With the pistons at the maximum stroke position, i.e. the pistons are expanded to S_1 in Figure 3, helium is fed into the system through valve V8. Since the total amount of gas in the system and the pressure P3 are known the amount of gas in the *column side* can be calculated from the mass balance. Thus the volume can be calculated from the ideal gas law. By slowly moving the pistons a known distance the variable volume of the piston can be calculated. The pistons are moved slowly, i.e.$v_p = 10\, mm/s$, to minimise friction and expansion temperature effects. According to the ideal gas law the piston volume and the volume from V8 to the fully expanded pistons are averaged to be $V_p = (2.0 \pm 0.2) \cdot 10^{-4} m^3$ and $V_{V8-p} = (5.4 \pm 0.2) \cdot 10^{-5} m^3$, respectively. The measured piston volume agrees with the volume calculated from the piston dimensions.

5.3 Resistance in the piston-column connection

By running the two pistons out-of-phase, i.e. the volume in the system is constant, the pressure drop between the two pistons can be measured. In the case of an empty column this pressure drop will be dominated by the pressure drop in the lines between the pistons and the column and thus allows the characterisation of the resistance in the piping. While the length and shape of the piping is slightly different for the two pistons the pressure drop is small and thus the same resistance is assumed for both pistons. The difference between the maximal and minimal pressure drops for He, N_2 and CO_2 and for different cycle times are given in Table 3. The pressure drop (DP1 in Figure *1*) has a small bias (<0.5 mbar) which varied slightly between experiments. It was decided to report the difference between the maximal and minimal pressure drop which will be twice the maximal pressure drop for a symmetric cycle.

Table 3: The difference between the maximal pressure drop and the minimal pressure drop for the empty

column run with full stroke at 303K and out-of-phase. Given is the mean value plus/minus the standard deviation if more than one experiment was run.

Cycle time [s]	max ΔP – min ΔP He [mbar]	max ΔP – min ΔP N_2 [mbar]	max ΔP – min ΔP CO_2 [mbar]
4	3.06±0.33	8.97±0.03	13.21
10	0.89±0.02	2.39±0.08	3.07
20	0.4	0.77±0.05	1.02

The experiments with He are in the laminar flow regime for all tested cycle times, while N_2 and CO_2 are in the turbulent flow regime for fast cycles (t_c=4s) and transition to the laminar regime between cycle times of 4 and 10 seconds. The pressure drop for He reduces roughly proportional to the increase in cycle time, which agrees with the standard model for pressure drop for laminar flow in pipes. The ratio of the pressure drops of N_2 and CO_2 for fast cycles is proportional to the ratio of their molecular weights, which also agrees with the standard model for pressure drop in pipes. However, for larger cycle times this relationship does not hold due to the transition from turbulent to laminar flow.

The experimental and simulated pressure profile for He for two different cycle times is given in Figure 5. The non-isothermal simulation from Section 3 shows excellent agreement with the experiments at slow and fast cycles. This agreement shows that the behaviour of the DP-PSA system for non-adsorbing gases can be predicted with high accuracy. Thus the behaviour for adsorbing gases can be used to investigate the mass and heat transfer characteristics of novel adsorbents.

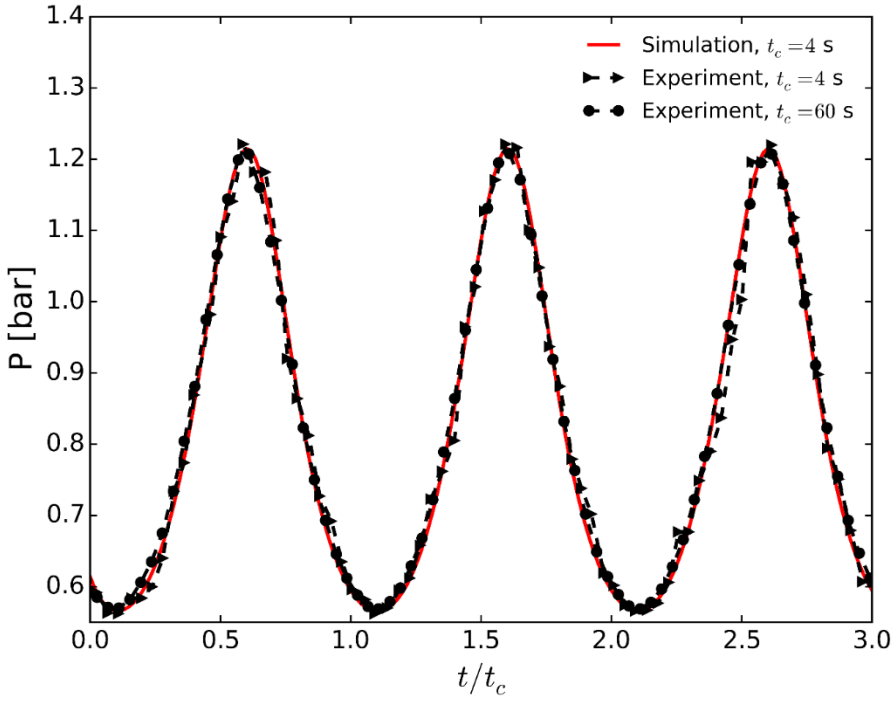

Figure 5: Experimental and simulated pressure profile for He in the empty column at two cycle times. The simulation for t_c=60s overlaps the one for t_c=4s. Conditions: T_0=30˚C; $\varphi = 0.5\pi$; Stroke1= Stroke2=0~75mm

5.4 System leak rates

Since the system is run in total reflux mode and several experiments are run sequentially it is important to

quantify the leak rate of the system. It is assumed that the leak rate is dependent on the pressure and a leak parameter K through the following leak rate differential equation

$$\frac{dn}{dt} = K(P_{atm} - P).$$

The parameter K is estimated by fitting the experimental pressure to the leak rate equation. Several experiments and fittings were performed for the three gases and spanning temperatures from 300 to 380 K and cycle times from 4 to 20s. The leak rate for these experiments varied between 3.5×10^{-8} and 12.4×10^{-8} mol s^{-1} bar^{-1} with no clear dependency on the gas composition, temperature or cycle time. While it would be preferable to match the leak rate to the specific experimental conditions, simulations with the average leak rate of 8×10^{-8} mol s^{-1} bar^{-1} are able to match the experimental data for simulations up to 3 hours with a relative error of less than 5%.

6. Packed column runs

After the characterisation of the empty DP-PSA system the column was packed with zeolite 13X pellets to show the capabilities and experimental procedure for the analysis of mass and heat transfer kinetics of adsorbents. The column was filled with 12.98 g of zeolite 13X pellets which have an average diameter of 4 mm, plus the two pellets on the thermocouples. The total sample mass was 13.1 g. First the system was run with He to measure the dead volume and the pressure drop along the column. This was followed by runs with N_2 and CO_2 with different cycle configurations.

6.1 Dead volume and void fractions of the system

The dead volume was determined similar to the procedure in section 5.2. Briefly, the *feed side* was filled with a known amount of He; the evacuated *column side* was filled from the *feed side*; the dead volume was calculated from the known volume on the *feed side* and the pressures on the *feed* and *column side*. The volume from V8 to the fully expanded pistons averaged over three experiments is $V_{V8-p} = 4.62 \cdot 10^{-5} m^3$. This value includes the volume of the column as well as the dead volume at the head of the pistons and in the lines connecting the column to the pistons. From this volume and the volume of the empty column the total void fraction is calculated as$\varepsilon_T = 0.77$. This allows the calculation of the inter-pellet void fraction ε from$\varepsilon_T = \varepsilon + (1-\varepsilon)(\varepsilon_p + (1-\varepsilon_p)\varepsilon_{cr})$. The crystal void fraction of zeolite 13X can be calculated from the framework and is $\varepsilon_{cr} = 0.5$[33]. The pellet void fraction is$\varepsilon_p = 0.25$. Thus the inter-pellet void fraction is $\varepsilon = 0.43$which is consistent with the result by de Klerk [34].

These void fractions enable the simulation of He runs in the packed column. Figure 6 shows experimental pressure profiles for He runs with different cycle times. The pressure profiles are normalised with respect to the pressure amplitude and the cycle time. P_0 is the average pressure for a given cycle. The normalised pressure profiles for different cycle times overlap almost perfectly. Also shown is the simulated pressure profile for one cycle time; the simulated pressure profiles for the other cycle times are almost exactly the same. The pressure curves are periodic and successive peaks have the same amplitude, which confirms that the leak rate of the system is small enough when the pistons are running. Furthermore, the experimental pressure profiles agree well with the simulated pressure profiles which validates the dimensions and dead volumes of the DP-PSA system used in the simulations.

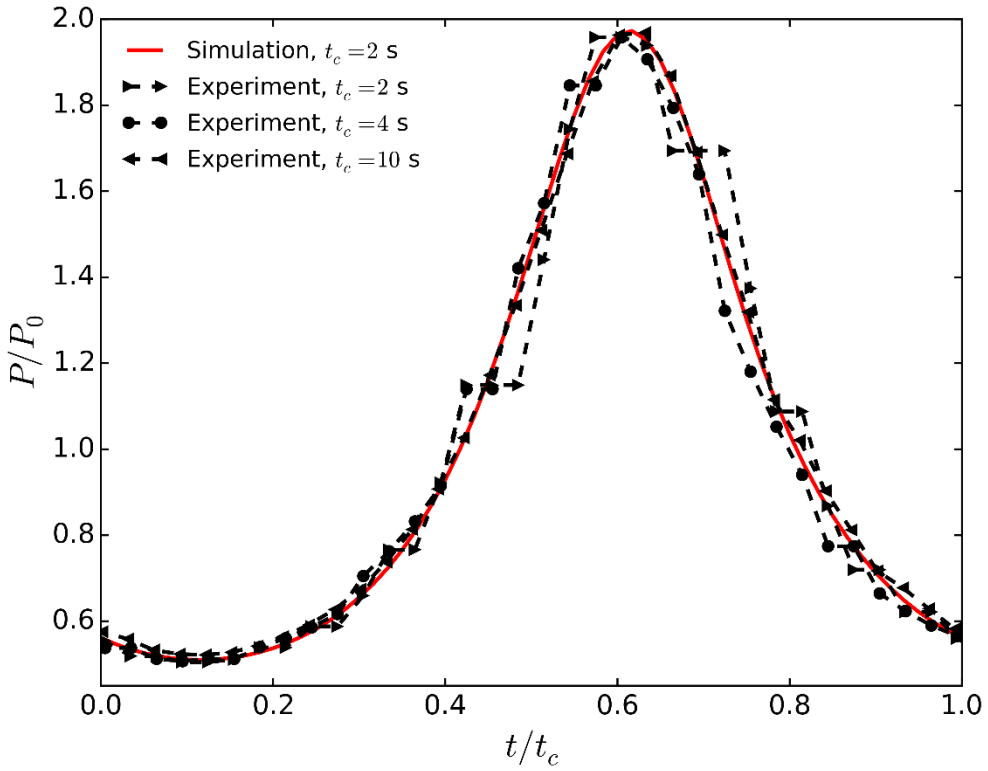

Figure 6: Experimental and simulated dimensionless pressure profile for He runs in the packed bed with different cycle times. Conditions: T_0=30˚C; $\varphi = 0.5\pi$; Stroke1= Stroke2=0~100mm

6.2 Pressure drop along the column

A differential pressure transducer connected to either end of the column allows the measurement of the pressure drop along the length of the column. Table 4 lists the difference between the maximal and minimal pressure drop for He, N_2 and CO_2 runs under different initial temperatures and cycle times when two pistons were run with a phase angle of φ=0.5π. The pressure drop is mainly affected by the flow velocity and the density of the gas. This is in agreement with the pressure drop calculated by the Ergun equation.

Table 4: The difference between the maximal and minimal pressure drop and the max pressure for the packed column run with full stroke and a phase angle of 0.5π

T [˚C]	t_c [s]	S [mm]	max P He [bar]	max ΔP – min ΔP He [mbar]	max P N_2 [bar]	max ΔP – min ΔP N_2 [mbar]	max P CO_2 [bar]	max ΔP – min ΔP CO_2 [mbar]
30	1	0-25	1.81	2.79				
30	4	0-100	1.96	3.56	1.58	7.77	1.983	11.67
30	10	0-100	1.89	0.91	1.83	2	1.924	2.55
60	4	0-100	1.68	3.26				
60	10	0-100	1.83	0.92				
100	4	0-100	1.64	3.17	1.82	7.07	1.916	10.29
100	10	0-100	1.78	0.89	1.73	1.57	1.958	2.09
100	20	0-100	1.74	0.36	1.7	0.73		

Figure 7 shows the pressure drop of CO_2 runs in the packed column for two different cycle times and a phase

offset of 0.5π between the two pistons. As expected the pressure drop of fast cycles is significantly larger than that of slower cycles in agreement with the dependency on the fluid velocity. This plot shows that there is good agreement between the simulation and experiment. Thus the Ergun pressure drop equation is sufficient for the accurate description of the pressure drop in the DP-PSA system.

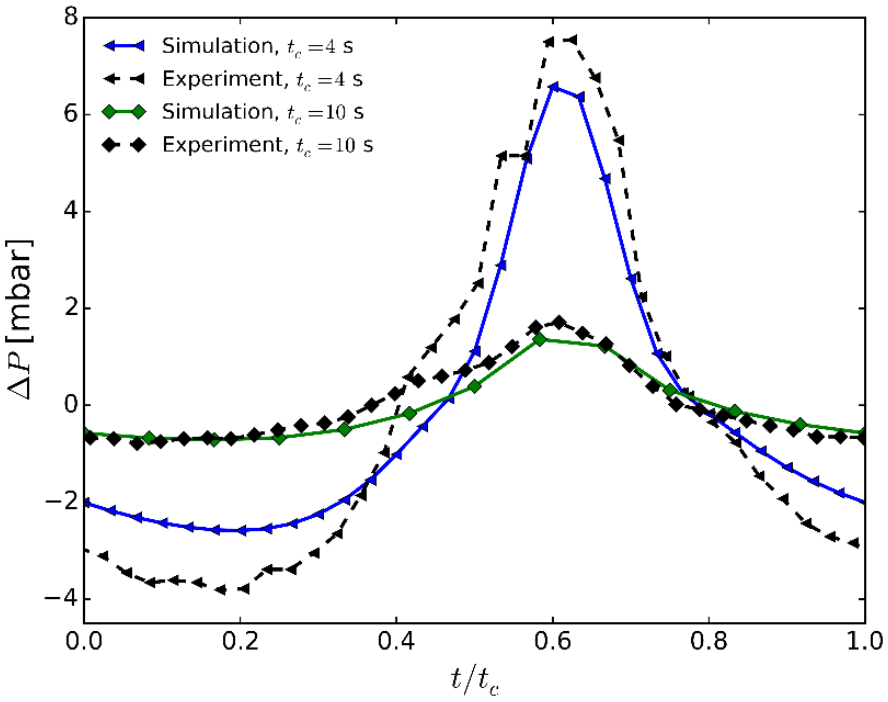

Figure 7: Pressure drop profiles for CO_2 runs in the packed bed with different cycle times. Conditions: T_0=30˚C; $\varphi = 0.5\pi$; Stroke1= Stroke2=0~100mm

Both the pressure drop and the absolute pressure (see Figure 6) are following an asymmetric profile. It was recently shown that this asymmetric pressure profile leads to a temperature gradient along the column due to the different amounts of work required for the compression in the two pistons [20].

6.3 Adsorbing gases in the packed column

Figure 8 shows the comparison of pressure profiles for CO_2 runs in the packed column for three different cycle times. Comparing the peak pressure at maximum compression shows the effect of the mass transfer resistance on the adsorption of CO_2. The maximum pressure among these experiments is decreasing with increasing cycle time. Experiments with cycle times larger than 20s showed the same response as seen from the cycle with t_c=40s. Thus the pressure profile for these slow cycles is not dependent on the kinetics but only on the adsorption isotherm. It is also interesting to note that the position of the pressure peak is shifted for the fast cycles.

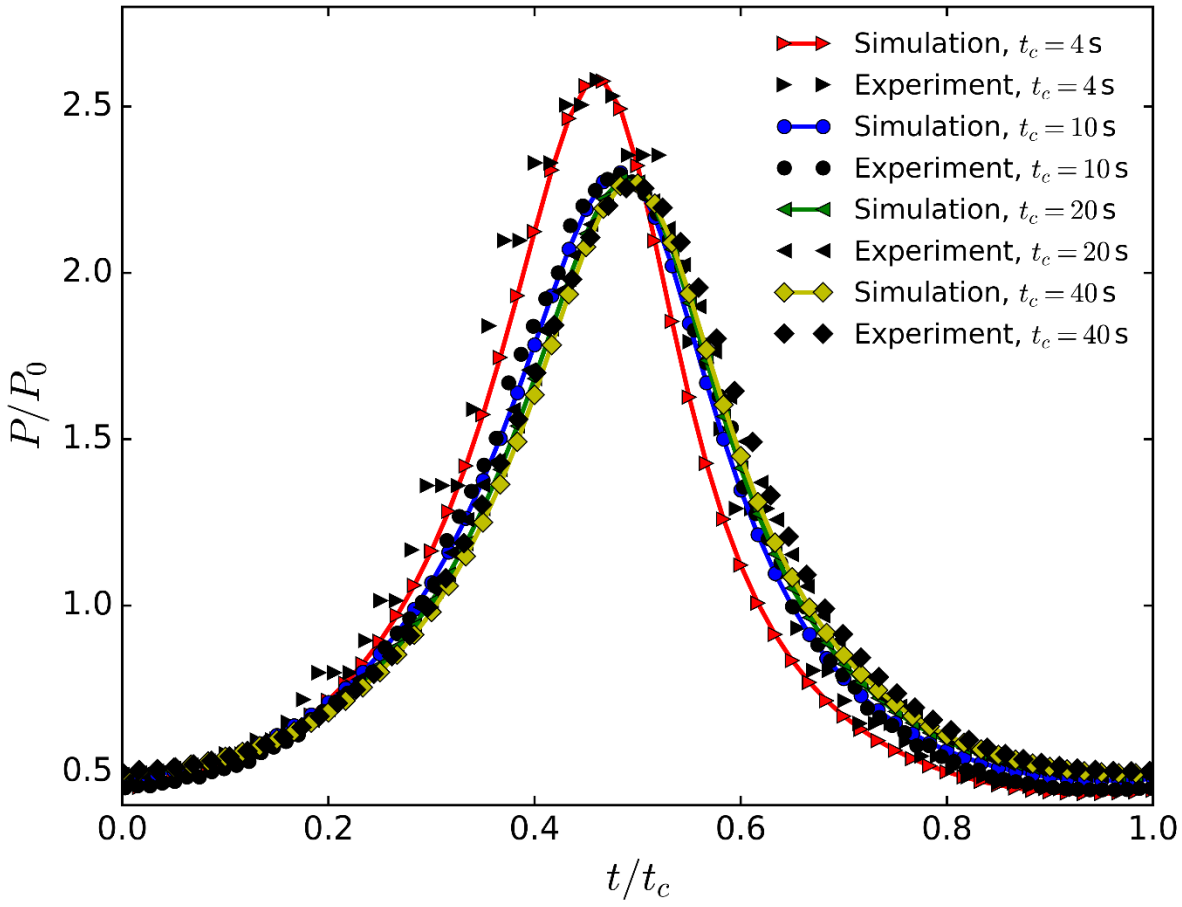

Figure 8: Comparison of the pressure profiles for the CO_2 runs in the packed bed with different cycle times. Conditions: T_0=30˚C; $\varphi = 0$; Stroke1= Stroke2=0~100mm

Figure 9 and Figure 10 show a comparison of the gas phase temperature profiles for a fast and slow cycle. It is crucial to take the heat transfer resistance in the thermocouple into account to have a fair comparison between the simulated profile and experimental profile which includes this resistance. The thermocouple temperature shown in these figures is calculated from the simulated pellet temperature with Eq. 27. The heat transfer coefficient to the thermocouple is limited by the solid heat conductivity and the other heat transfer coefficients are calculated from the Nusselt number correlations (23)-(26). For the fast cycles (t_c<10s) the Nusselt numbers need to be increased by 60% to be able to match the pressure and temperature data. This is due to the increasingly turbulent and oscillating flow [30]. Furthermore, the slower cycle shows a larger temperature swing compared to the faster cycle, i.e. around 16 K compared to around 12 K. This is due to the increased amount of adsorption at the slower cycle. The measured temperature swing in the fast cycle is even lower due to the short cycle time and the limited heat transfer to the thermocouple.

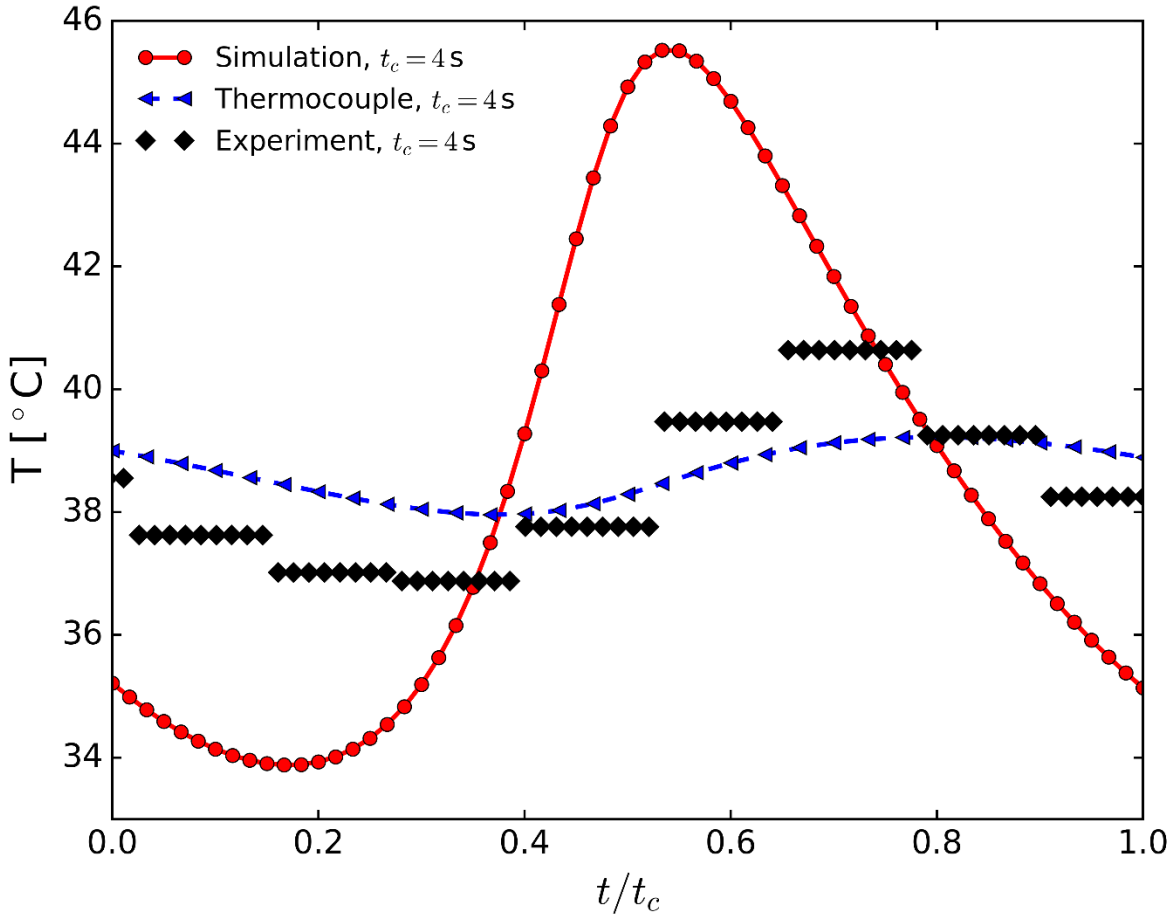

Figure 9: Solid temperature profile for a CO_2 run in the packed bed. The solid line shows the simulated temperature in the solid phase while the dashed line shows the thermocouple temperature calculated from Eq. 27. Conditions: T_0=30˚C; $\varphi = 0$; Stroke1= Stroke2=0~100mm; t_c=4s

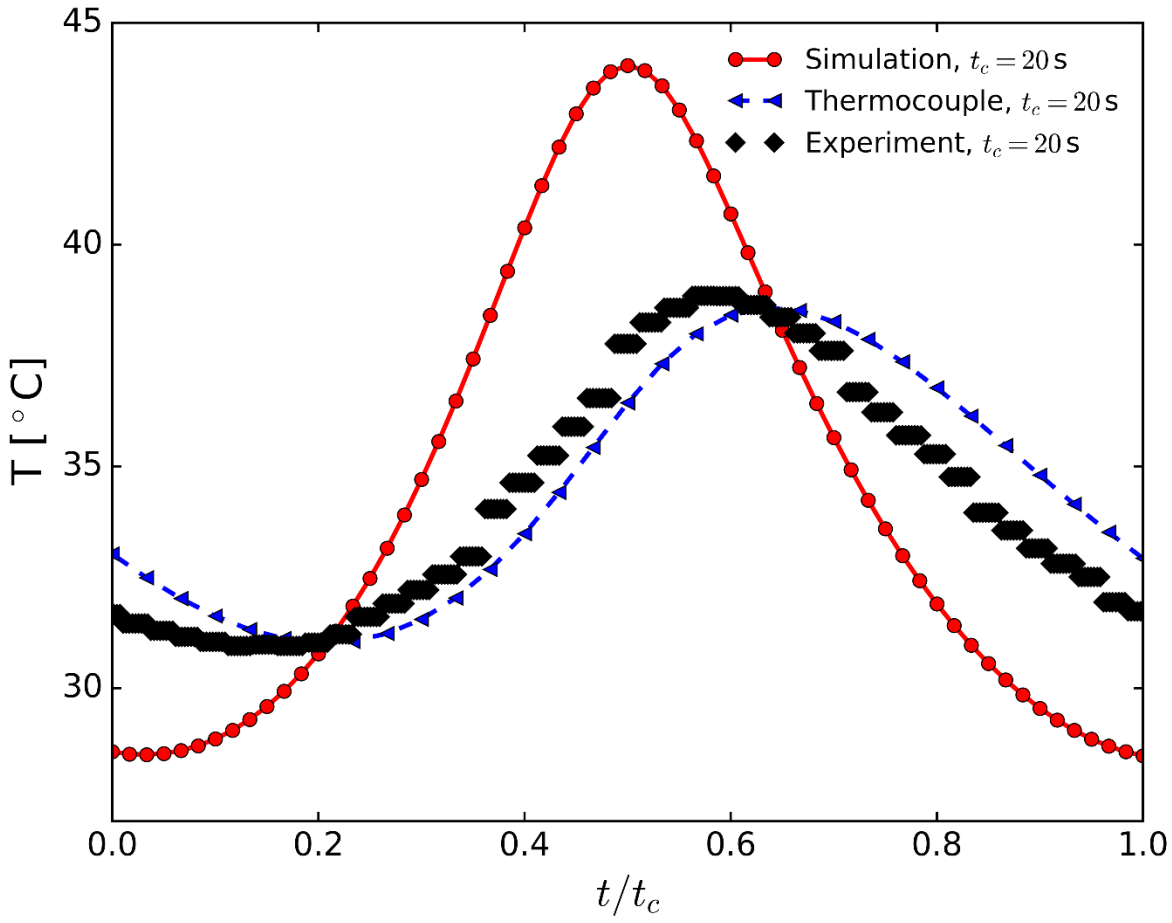

Figure 10: Solid temperature profile for a CO_2 run in the packed bed. The solid line shows the simulated temperature in the solid phase while the dashed line shows the thermocouple temperature calculated from Eq. 27. Conditions: T_0=30˚C; $\varphi = 0$; Stroke1= Stroke2=0~100mm; t_c=20s

Figure 11 shows the normalised pressure profile for experiments with the same cycle conditions but with different gases. As expected the amplitude of the pressure fluctuations follows the inverse order of the adsorption strength, i.e. He > N_2> CO_2. Besides this reduction in pressure amplitude for increasing adsorption strength it is interesting to note the shift of the pressure peak to earlier times for stronger adsorbing gases. While the pressure peak for He coincides with the time of the lowest volume (due to the phase shift the lowest volume is reached for t=0.625t_c) this is not true for CO_2 and to some extent also for N_2. This shift in the pressure peak is due to the interplay between the rate of volume decrease and the mass transfer kinetics: the rate of volume change decreases close to the minimum volume and the adsorption is able to compensate the volume decrease which leads to the shift in pressure peak. This kinetic effect is responsible for the non-symmetric pressure profiles of CO_2 and N_2 and reduces with increasing cycle time.

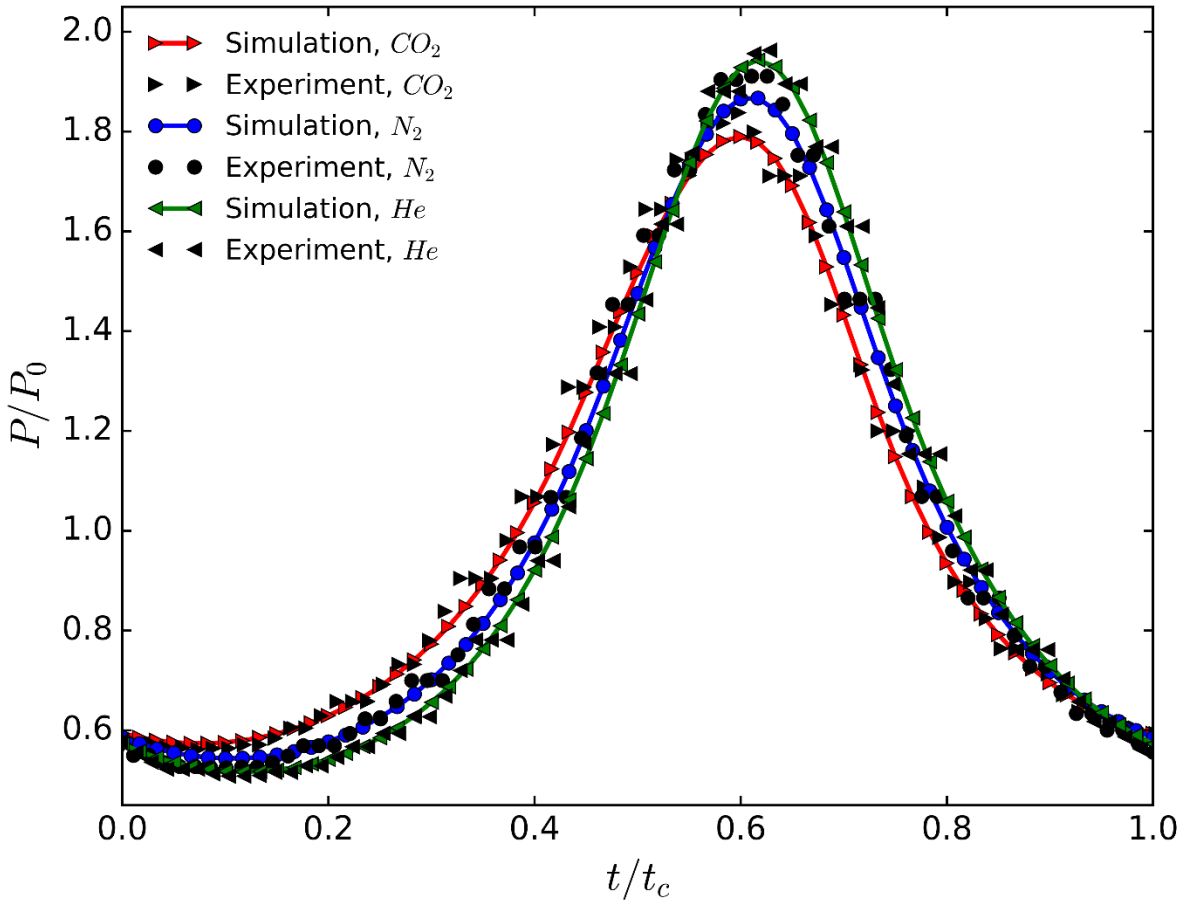

Figure 11: Comparison of the pressure profiles for runs in the packed bed with different gases. Conditions: T_0=30˚C; $\varphi = 0.5\pi$; Stroke1= Stroke2=0~100mm; t_c=4s.

6.4 Experimental accuracy and sensitivity to equilibrium and mass transfer parameters

To use the DP-PSA system to evaluate adsorbents, we need to characterise the system accuracy. Figure 12 shows the cycle pressure averaged over 100 cycles for two independent experimental runs with almost the same cycle configuration. We interpolate all experimental points with the cubic spline method so that we can compare measured values over the 100 cycles. The small difference at the pressure peak is due to a slightly higher charge pressure for run 2 which leads to higher adsorption and thus lower normalised pressure peak. By taking this small difference into account, we can match both experimental curves accurately with the same adsorbent parameters. The 99% confidence interval for the experimentally measured pressure is shown in the dotted lines which almost coincide with the average pressure.

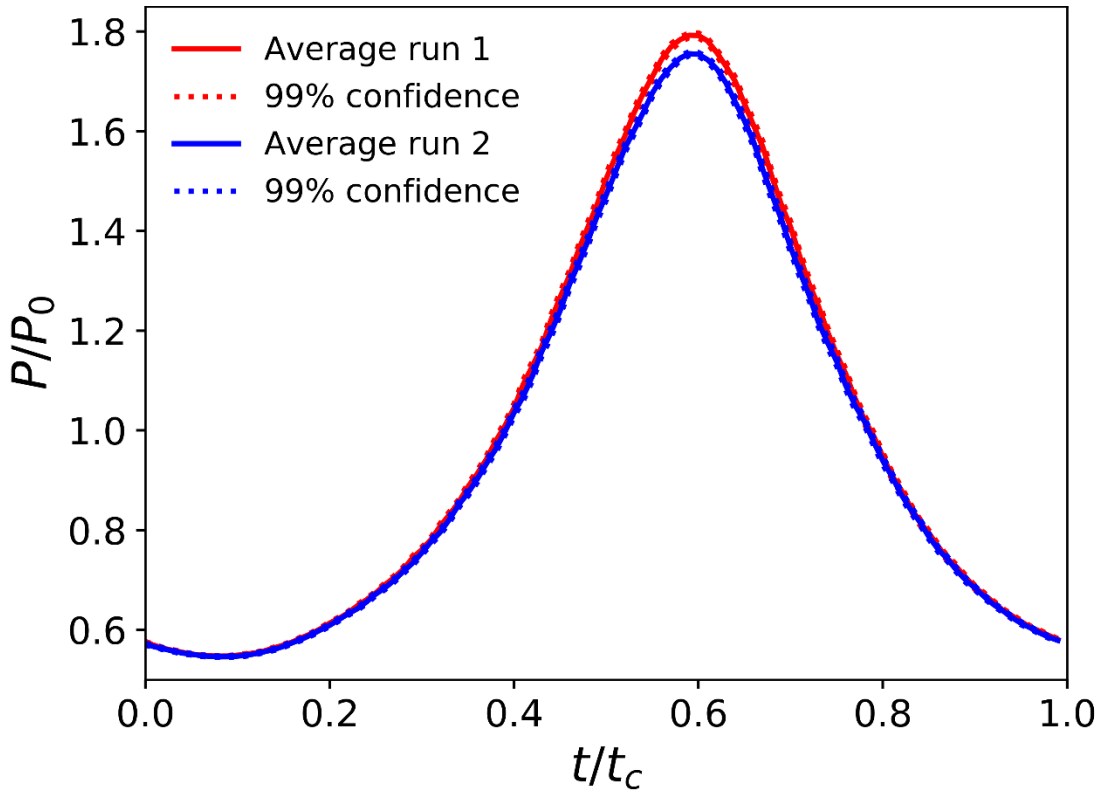

Figure 12: Average experimental pressure and 99% confidence interval for two independent CO_2 experimental runs. The only difference between run 1 and run 2 is that the two pistons are swapped, i.e. run 1 has $\phi=0.5\pi$ and run 2 has $\phi=1.5\pi$. Conditions: T0=30˚C; $\phi=0.5\pi$; Stroke1= Stroke2=0~100mm, tc=4s.

While in this contribution both equilibrium and mass transfer parameters have been taken from previous studies on commercial 13X beads, here we show briefly what is the effect of a 10% uncertainty on the DP-PSA response. We increase the equilibrium saturation capacities of both sites and the effective macropore diffusivities by 10% to test uncertainty in the isotherm and kinetics, respectively. First we consider the case of a relatively slow cycle, t_c=20s. Figure 13 shows clearly that a 10% increase in the equilibrium adsorbed amount has a direct effect on the pressure response for CO_2, while kinetics are fast enough so that at this cycle time there is no discernible effect.

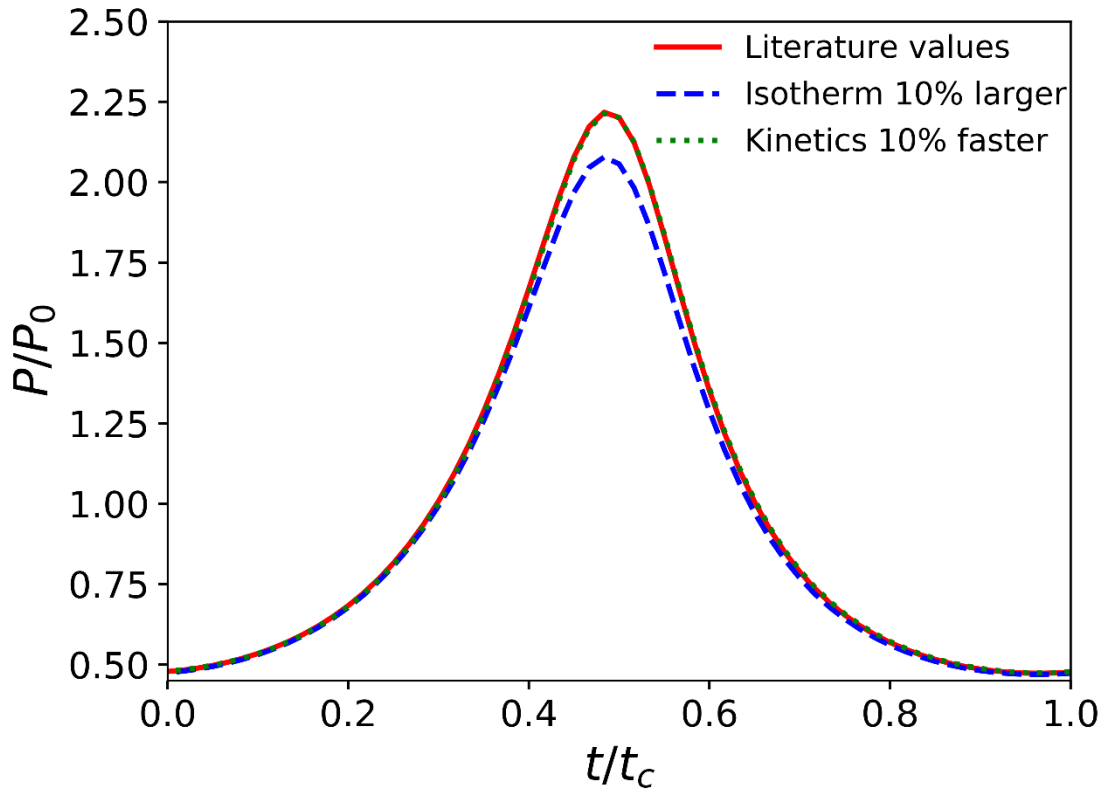

Figure 132: Pressure profiles of the CO_2 simulation runs in the packed bed with different isotherm and kinetic parameters. Conditions: T0=30˚C; ϕ=0; Stroke1= Stroke2=0~100mm, t_c=20s.

Figure 14 and 15 show the same comparison for a fast cycle, t_c=4s. Here we see that the change in equilibrium adsorbed amount has a reduced effect. This is due to the competing effects of the larger equilibrium constant which in turn reduces the effective macropore diffusion. At this faster cycle the faster kinetics has an appreciable effect, which can be seen more clearly in the temperature response, where both the amplitude and phase lag are directly affected. The increased sensitivity of the temperature response is consistent with the observations in ref. [10]. This points to the potential improvement of the DP-PSA system by using thermocouples with faster dynamic response, but there is a trade-off between being able to seal the system minimizing leaks (the current thermocouples allow the use of standard Swagelok fittings) and the use of very thin thermocouples which are more difficult to insert inside the column and are potentially less robust.

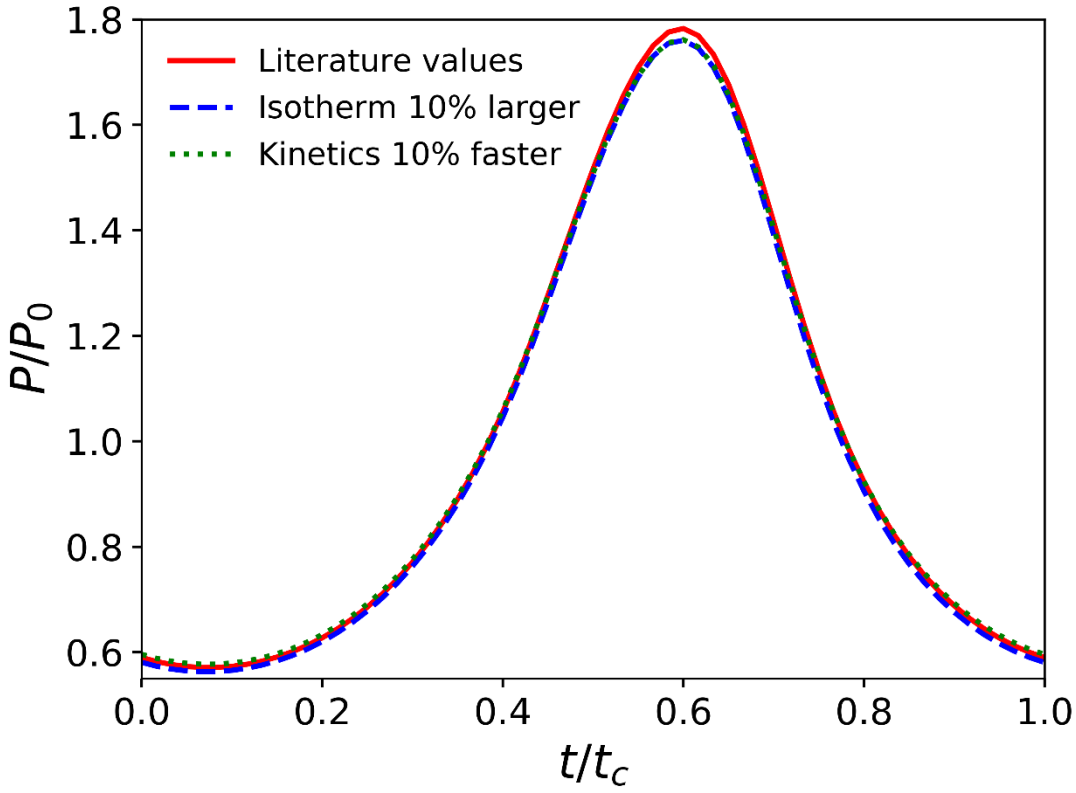

Figure 14: Pressure profiles of the CO_2 simulation runs in the packed bed with different isotherm and kinetic parameters. Conditions: T0=30˚C; ϕ=0.5π; Stroke1= Stroke2=0~100mm, t_c=4s.

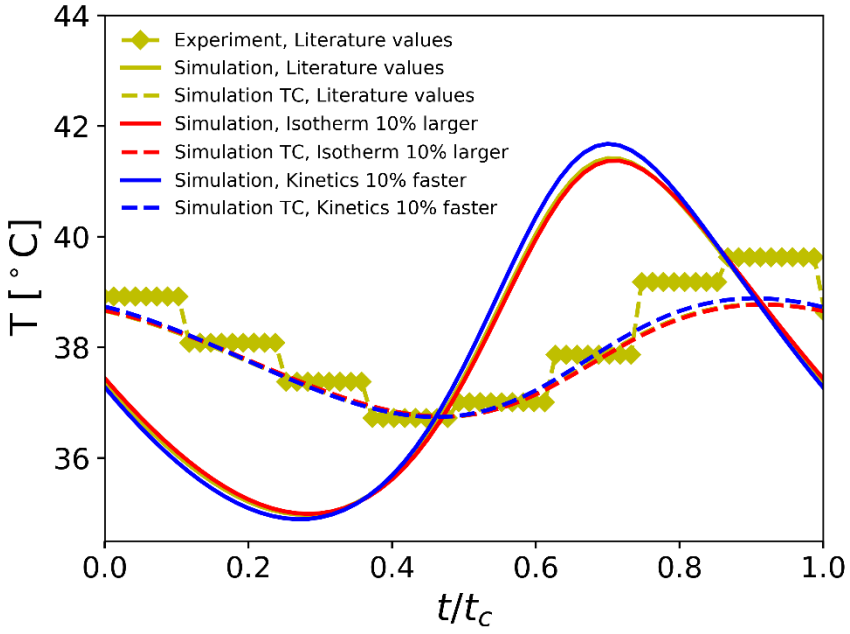

Figure 15: Temperature profiles of the CO_2 simulation runs in the packed bed with different isotherm and

kinetic parameters. Conditions: T0=30˚C; ϕ=0.5π; Stroke1= Stroke2=0~100mm, tc=4s.

7. Conclusions

Here the characterisation and operation of the Dual Piston Pressure Swing Adsorption system as well as a non-isothermal mathematical model for the analysis of the experimental runs are presented. DP-PSA systems are uniquely suited to test novel adsorbents due to a wide range of operating conditions which allow the probing of different experimental regimes. The semi-automatic DP-PSA system described in this contribution has two pistons which are independently controlled through a LabVIEW interface. In contrast to previous systems this enables the automated and autonomous running of a large number of experiments which is essential for the testing of novel adsorbents. The LabVIEW control code is deployed to a Compact RIO real-time computer which also handles the logging of the actual piston position as well as the system pressures and temperatures. A series of experiments with different cycle configurations, e.g. cycle time and stroke length, is defined in a graphical interface and the experiments are run independently on the real-time computer. This allows the testing of adsorbent materials under different experimental conditions such as different pressure ratios and cycle times. Therefore, this system is particularly suitable to measure kinetic and equilibrium properties of novel adsorbent materials. Furthermore, this automation increases the reliability and accuracy of the cycle control and data logging. The control code and data logging enables the running of smooth sinusoidal piston cycles with cycle times smaller than 1s. These fast cycles are critical in the characterisation of adsorbent for rapid PSA processes which can achieve a higher productivity and lower costs compared to conventional PSA cycles.

The empty DP-PSA system and the mathematical model were characterised with He experiments. This characterisation showed that the computer controlled pistons can generate a smooth sinusoidal cycle profile similar to the earlies mechanical DP-PSA systems. Furthermore, the system has a low leak rate which enables the automated running of a series of experiments. Finally, in contrast to a previous DP-PSA system, the semi-automated system has a very low flow resistance between the pistons and the column. This characterisation of the system is crucial to account for these effects in the analysis of adsorbents.

The experimental procedure for the analysis of novel adsorbents was demonstrated with the analysis of the adsorption of CO_2 on zeolite 13X pellets. First, the void fraction and the pressure drop along the column were quantified with He runs. This is followed by a series of experiments with CO_2. In this series the system is operated under different cycle times and oven temperatures. These experimental conditions were simulated with the adsorption isotherm and mass transfer kinetics of CO_2 on zeolite 13X previously measured. All parameters for these simulations are taken from the literature, except the void fraction which was measured previously. Only the Nusselt numbers for steady flow are slightly increased to account for the oscillatory nature of the flow. The experimental and simulated pressure and temperature profiles showed excellent agreement. This shows that the mathematical model and, in particular, the heat transfer correlations are suitable for the analysis of adsorbents.

These results confirm the feasibility of this apparatus for the characterisation of novel adsorbent materials. While this system can generate a large amount of experimental data at different conditions, it is essential to develop an efficient parameter estimation method to extract the isotherm and mass transfer parameters. The development of such a tool will be detailed in a future publication.

Nomenclature

A	Surface area, m^2
$b_{i,0}^{l}$	Langmuir constant of comp. i for site l, bar^{-1}
c_i	Concentration of comp. i in the gas phase, $mol\ \ m^{-3}$
$\hat{c}_P$	Specific heat capacity, $J\ \ kg^{-1}\ \ K^{-1}$
c_T	Total concentration in the gas phase, $mol\ \ m^{-3}$
D	Diffusion coefficient, $m^2\ \ s^{-1}$
F	Molar flow rate, $mol\ \ s^{-1}$
h	Heat transfer coefficient, $W\ \ m^{-2}\ \ K^{-1}$
$\breve{H}$	Enthalpy per unit volume, $J\ \ m^{-3}$
$\widetilde{H_i}$	Partial molar enthalpy of component i, $J\ \ mol^{-1}$
ΔH_i^l	Heat of adsorption of comp. i at site l, $mol\ \ m^{-2}\ \ s^{-1}$
J_i	Diffusive flux of comp. i, $mol\ \ m^{-2}\ \ s^{-1}$
J_{th}	Thermal diffusive flux of comp. i, $mol\ \ m^{-2}\ \ s^{-1}$
k	Thermal conductivity, $J\ \ m^{-1}\ \ s^{-1}\ \ K^{-1}$
k_i	LDF mass transfer coefficient of comp. i, m s^{-1}
L	Length, m
Nu	Nusselt number
P	Pressure, bar
Pr	Prandtl number
$\overline{q_i}$	Sorbate concentration of comp. i averaged over the adsorbent crystal, $mol\ \ m^{-3}$
q_i^*	Sorbate concentration of comp. i at equilibrium, $mol\ \ m^{-3}$
$\overline{Q_i}$	Concentration of comp. i averaged over the adsorbent pellet, $mol\ \ m^{-3}$
r	Radius, m
R	Gas constant, $J\ \ mol^{-1}\ \ K^{-1}$
Re	Reynolds number
S	Piston position, m
Sc	Schmidt number
t	Time, s
T	Temperature, K
U	External heat transfer coefficient, $W\ \ m^{-2}\ \ K^{-1}$
U	Internal energy, J
$\breve{U}$	Internal energy per unit volume, $J\ \ m^{-3}$
V	Volume, m^3
x_i	Mole fraction of comp. i in the gas phase
z	Axial distance, m
Greek symbols	
ε	Void fraction
κ	Flow resistance, $mol\ \ s^{-1}\ \ bar^{-1}$
λ	Thermal conductivity, $J\ \ m^{-1}\ \ s^{-1}\ \ K^{-1}$
μ	Viscosity, $Pa\ \ s$
ρ	Density, $kg\ \ m^{-3}$
τ	Tortuosity
φ	Initial piston offset
ω	Cycle frequency, s^{-1}
Subscript	

c	Column
cr	Crystal
e	External
f	Fluid phase
i	Internal
L	Axial direction
m	Macropore
n	Neighbouring unit
o	Outside the piston
p	Pellet
s	Saturation
th	Thermal
T	Total
TC	Thermocouple
w	Wall
∞	Surroundings
Superscript	
cr	Crystal
e	Effective
K	Knudsen
L	Axial direction
m	Molecular
p	Pellet
v	Viscous

Appendix

The Reynolds number is

$$Re = \frac{2rv\rho}{\mu} = \frac{2rF\mathrm{MW}}{\epsilon A\mu}$$

where F is the molar flow rate, MW is the molecular weight of the gas mixture, ϵ is the void fraction, A is the cross-sectional area and μ is the dynamic viscosity. The radius in the numerator depends on the relevant length scale. For the connecting pipes it is the pipe radius and for the pellet it is the pellet radius. For the column Reynolds number it depends on the packing of the column: the empty column behaves like a pipe and the relevant length scale is the column radius; for the packed column the pellet radius is the relevant length scale. Thus the Reynolds numbers are for the connecting pipe

$$Re_{pipe} = \frac{2r_{pipe}F\mathrm{MW}}{\pi r_{pipe}^2\mu}$$

for the pellet

$$Re_p = \frac{2R_pF\mathrm{MW}}{\epsilon\pi r_c^2\mu}$$

and for the column

$$Re_c = \frac{2r_cF\mathrm{MW}}{\epsilon\pi r_c^2\mu}, \qquad \text{for } \epsilon \approx 1$$

$$Re_c = \frac{2r_pF\mathrm{MW}}{\epsilon\pi r_c^2\mu}, \qquad \text{otherwise.}$$

Gas	Adsorbent	Po	P1 S0	P2 S0	P1 S1	P2 S1	P1 (S1-S0)	P2 (S1-S0)	T	Cycle time	Phase angle	Figure
		bar	mm	mm	mm	mm	mm	mm	°C	s		
He	13X (2pellets)	0.81	0	0	75	75	75	75	30	4	0.5π	5
He	13X (2pellets)	0.82	0	0	75	75	75	75	30	60	0.5π	5
He	13X (packed)	0.85	0	0	100	100	100	100	30	2	0.5π	6
He	13X (packed)	0.94	0	0	100	100	100	100	30	4	0.5π	6, 11
He	13X (packed)	0.95	0	0	100	100	100	100	30	10	0.5π	6
CO2	13X (packed)	1.14	0	0	100	100	100	100	30	**4**	0.5π	7, 11, 12, 14, 15
CO2	13X (packed)	1.24	0	0	100	100	100	100	30	4	1.5π	12
CO2	13X (packed)	1.23	0	0	100	100	100	100	30	10	0.5π	7
CO2	13X (packed)	1.01	0	0	100	100	100	100	30	4	0	8, 9
CO2	13X (packed)	1.32	0	0	100	100	100	100	30	10	0	8
CO2	13X (packed)	1.31	0	0	100	100	100	100	30	20	0	8, 10, 13
CO2	13X (packed)	1.31	0	0	100	100	100	100	30	40	0	8
N2	13X (packed)	1.03	0	0	100	100	100	100	30	4	0.5π	11

Supplementary table 1: Experimental runs shown in the figures

References

[1] J. C. Abanades *et al.*, "Emerging CO2 capture systems," *Int. J. Greenh. Gas Control*, vol. 40, pp. 126–166, 2015.

[2] D. M. D'Alessandro, B. Smit, and J. R. Long, "Carbon dioxide capture: Prospects for new materials," *Angew. Chemie - Int. Ed.*, vol. 49, no. 35, pp. 6058–6082, 2010.

[3] J. Yang, M. Park, J. Chang, S. Ko, and C. Lee, "Effects of pressure drop in a PSA process," *Korean J. Chem. Eng.*, vol. 15, no. 2, pp. 211–216, 1998.

[4] S. Hayashi, M. Kawai, and T. Kaneko, "Dynamics of high purity oxygen PSA," *Gas Sep. Purif.*, vol. 10, no. 1, pp. 19–23, 1996.

[5] D. M. Ruthven, *Principles of adsorption and adsorption processes*. Wiley-Interscience, 1984.

[6] G. E. Keller and C. H. A. Kuo, "United States Patent 4354859," 1982.

[7] Y. Yasuda, "Frequency Response Method for Study of the Kinetic Behavior of a Gas-Surface System. 1. Theoretical Treatment," *J. Phys. Chem.*, vol. 80, no. 17, pp. 1867–1869, 1976.

[8] Y. Yasuda, "Frequency-Response method for investigation of gas-surface dynamic phenomena," *Heterog. Chem. Rev.*, vol. 1, no. 2, pp. 103–124, 1994.

[9] L. V. C. Rees and D. Shen, "Characterization of microporous sorbents by frequency-response methods," *Gas Sep. Purif.*, vol. 7, no. 2, pp. 83–89, 1993.

[10] V. Bourdin, L. M. Sun, P. Grenier, and F. Meunier, "Analysis of the temperature frequency response for

diffusion in crystals and biporous pellets," *Chem. Eng. Sci.*, vol. 51, no. 2, pp. 269–280, 1996.

[11] D. Brzić and M. Petkovska, "Nonlinear Frequency Response measurements of gas adsorption equilibrium and kinetics: New apparatus and experimental verification," *Chem. Eng. Sci.*, vol. 132, pp. 9–21, 2015.

[12] H. A. Boniface and D. M. Ruthven, "Chromatographic adsorption with sinusoidal input," *Chem. Eng. Sci.*, vol. 40, no. 11, pp. 2053–2061, 1985.

[13] Y. Wang and M. D. LeVan, "Mixture diffusion in nanoporous adsorbents: Development of Fickian flux relationship and concentration-swing frequency response method," *Ind. Eng. Chem. Res.*, vol. 46, no. 7, pp. 2141–2154, 2007.

[14] B. K. Sward and M. D. LeVan, "Frequency response method for measuring mass transfer rates in adsorbents via pressure perturbation," *Adsorpt. Int. Adsorpt. Soc.*, vol. 9, no. 1, pp. 37–54, 2003.

[15] D. M. Ruthven, S. Farooq, and K. S. Knaebel, *Pressure Swing Adsorption*. New York: VCH Publishers, 1994.

[16] K. Singh and J. Jones, "Numerical simulation of air separation by piston-driven pressure swing adsorption," *Chem. Eng. Sci.*, vol. 52, no. 18, pp. 3133–3145, Sep. 1997.

[17] R. Arvind, S. Farooq, and D. M. Ruthven, "Analysis of a piston PSA process for air separation," *Chem. Eng. Sci.*, vol. 57, pp. 419–433, Feb. 2002.

[18] S. Farooq, C. Thaeron, and D. M. Ruthven, "Numerical simulation of a parallel-passage piston-driven PSA unit," *Sep. Purif. Tech.*, vol. 13, pp. 181–193, 1998.

[19] D. Friedrich, M.-C. Ferrari, and S. Brandani, "Efficient simulation and acceleration of convergence for a Dual Piston Pressure Swing Adsorption system," *Ind. Eng. Chem. Res.*, vol. 52, pp. 8897–8905, 2013.

[20] W. Dang, D. Friedrich, and S. Brandani, "Characterisation of an automated Dual Piston Pressure Swing Adsorption (DP-PSA) system," *Energy Procedia*, vol. 37, pp. 57–64, Jan. 2013.

[21] X. Hu, S. Brandani, A. I. Benin, and R. R. Willis, "Development of a Semiautomated Zero Length Column Technique for Carbon Capture Applications: Rapid Capacity Ranking of Novel Adsorbents," *Ind. Eng. Chem. Res.*, vol. 54, no. 26, pp. 6772–6780, 2015.

[22] C. Sereno and A. E. Rodrigues, "Can steady-state momentum equations be used in modelling pressurization of adsorption beds?," *Gas Sep. Purif.*, vol. 7, no. 3, pp. 167–174, 1993.

[23] A. C. Hindmarsh *et al.*, "Sundials: Suite of Nonlinear and Differential/Algebraic Equation Solvers," *ACM Trans. Math. Softw.*, vol. 31, no. 3, pp. 363–396, Sep. 2005.

[24] X. Hu, E. Mangano, D. Friedrich, H. Ahn, and S. Brandani, "Diffusion mechanism of CO2 in 13X zeolite beads," *Adsorption*, vol. 20, no. 1, pp. 121–135, Jun. 2014.

[25] D. Friedrich, E. Mangano, and S. Brandani, "Automatic estimation of kinetic and isotherm parameters from ZLC experiments," *Chem. Eng. Sci.*, vol. 126, pp. 616–624, 2015.

[26] S. Whitaker, "Forced Convection Heat Transfer Correlations for Flow In Pipes, Past Flat Plates, Single Cylinders, Single Spheres, and for Flow in Packed Beds and Tube Bundles," *AIChE J.*, vol. 18, no. 2, pp. 361–371, 1972.

[27] E. N. Sieder and G. E. Tate, "Heat Transfer and Pressure Drop of Liquids in Tubes," *Ind. Eng. Chem.*, vol. 28, pp. 1429–1435, 1936.

[28] N. Wakao, S. Kaguei, and T. Funazkri, "Effect of fluid dispersion coefficients on particle-to-fluid heat transfer coefficients in packed beds: correlation of Nusselt numbers," *Chem. Eng. Sci.*, vol. 34, pp. 325–336, 1979.

[29] C.-H. Li and B. A. Finlayson, "Heat transfer in packed beds - a reevaluation," *Chem. Eng. Sci.*, vol. 32, pp. 1055–1066, 1977.

[30] J. E. Dec, J. O. Keller, and V. S. Arpaci, "Heat transfer enhancement in the oscillating turbulent flow of a

pulse combustor tail pipe," *Int. J. Heat Mass Transf.*, vol. 35, no. 9, pp. 2311–2325, 1992.

[31] K. Chan, C. Y. H. Chao, and M. Bahrami, "Heat and Mass Transfer Characteristics of a Zeolite 13X/CaCl2 Composite Adsorbent in Adsorption Cooling Systems," in *Proceedings of the ASME 2012 6th International Conference on Energy Sustainability & 10th Fuel Cell Science, Engineering and Technology Conference*, 2012, pp. 1–10.

[32] N. Wakao and T. Funazkri, "Effect of fluid dispersion coefficients on particle-to-fluid mass transfer coefficients in packed beds: correlation of Sherwood numbers," *Chem. Eng. Sci.*, vol. 33, pp. 1375–1384, 1978.

[33] J. Zhang, P. a. Webley, and P. Xiao, "Effect of process parameters on power requirements of vacuum swing adsorption technology for CO2 capture from flue gas," *Energy Convers. Manag.*, vol. 49, no. 2, pp. 346–356, 2008.

[34] A. de Klerk, "Voidage variation in packed beds at small column to particle diameter ratio," *AIChE J.*, vol. 49, no. 8, pp. 2022–2029, Aug. 2003.